TECHNICAL RESEARCH REPORT

An Orthogonal Collocation Technique for Rapid Thermal Processing System Discretization

by R.A. Adomaitis

T.R. 97-63

*Sponsored by
the National Science Foundation
Engineering Research Center Program,
the University of Maryland,
Harvard University,
and Industry*

An Orthogonal Collocation Technique for Rapid Thermal Processing System Discretization

Raymond A. Adomaitis
Department of Chemical Engineering and
Institute for Systems Research
University of Maryland, College Park MD 20742

July 8, 1997

Topical heading: Process Systems Engineering

Keywords: Orthogonal collocation; Rapid thermal processing; Model reduction

Abstract

A model of a multiple heating zone Rapid Thermal Processing (RTP) system is developed to study wafer thermal dynamics during a processing cycle. The system is discretized with trial functions generated from the linearized wafer energy balance equation eigenfunctions, and careful analysis of the solution residual reveals a slow, but predictable, convergence rate. A modified set of trial functions is derived from a subset of the original eigenfunctions combined with the dominant modes identified by the Karhunen-Loéve expansion of the wafer temperature variance component that contributes most to the slow convergence. Since the wafer temperature variance is computed explicitly from an eigenfunction expansion solution of the linearized system with specified processing statistics, the collocation procedure effectively links RTP model reduction and simulation in one discretization procedure. The convergence rate of the modified collocation method is shown to be superior to collocation methods based on the original eigenfunction and polynomial sequences.

1 Introduction

This paper presents a collocation discretization technique developed in the context of simulating a Rapid Thermal Processing (RTP) system. In RTP systems, single semiconductor wafers are processed in a cold-

walled chamber with wafer heating provided by one or more incoherent lamp banks. This process is used, or has potential for use, in a number of semiconductor device fabrication steps (Larrabee, 1994; Lord, 1988; Moslehi, 1994; Roozeboom, 1993; Singer, 1993), but is known to suffer from spatially nonuniform wafer temperature profiles during the short (on the order of one minute) processing cycle.

Numerous simulation studies aimed at understanding or controlling wafer temperature uniformity have been conducted, and the variety of discretization techniques used to discretize the wafer temperature partial differential equation number almost as large. Simulation results based on finite difference discretizations in one, two, and three dimensions (Dilhac et al., 1995; Sorrell et al., 1992), finite elements (Cole et al., 1994), orthogonal collocation with Jacobi polynomial trial functions (Breedijk et al., 1993), and wafer temperature representations in terms of Bessel function expansions (Belikov and Friedland, 1995) have been reported. While many of these studies compare simulated temperature profiles to experimental measurements as a means of model verification, there has been little explicit discussion of discretization errors and the computational efficiency of the discretization methods.

Because of the complexity of some of the simulators developed and the computational expenses of performing simulations for process optimization and control, interest in developing reduced-order models from the high fidelity simulations has emerged (Aling et al., 1996; Theodoropoulou et al., 1996). These models are based on collecting "snapshots" of the RTP system at points in time during processing cycles designed to excite as many spatial temperature modes as possible, and processing them with the Proper Orthogonal Decomposition method (Sirovich, 1987) to determine the dominant temperature spatial modes. Because the original modeling equations are projected onto these modes with some type of weighted residual method, the reduced-order models have a predictive capability not found in models generated from purely empirical model identification schemes.

A common characteristic of the cited model reduction methods is that detailed simulations or highly resolved experimental measurements must be performed prior to generating the reduced order models. This paper considers the problem of generating an optimized set of trial functions *before* performing simulations with the nonlinear wafer thermal dynamics model. The overall procedure developed begins with determining an eigenfunction expansion solution to the linearized system. By treating the individual lamp power inputs as

normal, independent random variables with specified mean and variance, we examine the expected convergence behavior of the solution as a function of the number of terms used in the eigenfunction expansion. From this information we rearrange the eigenfunctions with the Karhunen-Loéve expansion (Fukunaga, 1990) to form a set of orthogonal trial functions which, when used in a collocation discretization technique, gives far superior convergence rates. It is important to stress that we compute the elements of the mode amplitude variance array *explicitly* using an eigenfunction expansion solution. While this procedure may be suboptimal with regard to capturing features made important by system nonlinearities, its advantage is that the trial functions are generated prior to any nonlinear simulations. The method works because the nonlinearities of the RTP system, while significant, do not result in bifurcations or dynamical behavior that would have significant impact on the relative importance of different spatial modes (Graham and Kevrekidis, 1996).

The paper's focus on developing efficient collocation schemes was motivated by the natural connection between interpreting simulation results from discrete-ordinate models with measuring wafer temperatures at discrete points, and by the ease with which collocation methods are applied to discretizing nonlinear problems with nonlinear boundary conditions. The techniques developed in this work build on the collocation methods based on trial functions other than polynomials (see, e.g., Guertin et al., 1977; Sørensen and Stewart, 1982). The previous collocation studies based trial function selection on rules developed for the individual problems solved. The method described in this paper has potential for generating efficient trial functions for a wide range of boundary value problems.

2 RTP System Model

Consider the problem of modeling the spatially varying wafer temperature dynamics of an RTP system where the wafer is heated by three individually controllable heating lamp banks. A representative furnace design is shown in Fig. 1; this heating lamp bank configuration was patterned after the three-zone system RTP system of Kiether et al. (1994). A relatively simple model is developed here (c.f., Breedijk et al., 1993; Merchant et al., 1996; Theodoropoulou et al., 1996) so accurate residual calculations can be performed. The model is based on the following assumptions:

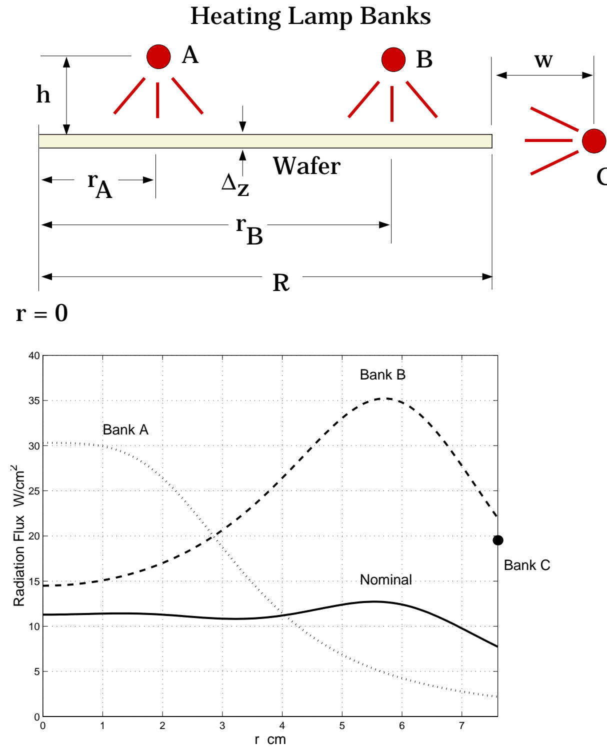

Figure 1: The dimensions of a three-zone RTP system (top) and the computed radiant flux distributions at the wafer surface $Q^A(r)$, $Q^B(r)$, and Q^C (bottom).

1. The wafer thermal conductivity k and heat capacity C_p are not functions of temperature;
2. Wafer temperature does not vary with z (thin wafer assumption);
3. The wafer is round (no chord), and azimuthal lamp radiation flux and wafer temperature variations are negligible;
4. The process operates at low pressure and sufficiently low deposition rates so that heat transfer to the process gas and contribution of heat of chemical reaction are negligible compared to the radiation emitted from the wafer and absorbed from the heating lamps; and
5. Radiation is emitted from both wafer sides and the wafer edge to a blackbody enclosure (the RTP chamber) maintained at T_{amb} in this cold-walled process.

Defining the dimensionless temperature T, radial position r, and time t as

$$T = \frac{T^*}{T_{\text{amb}}} \qquad r = \frac{r^*}{R} \qquad t = \frac{t^*}{t_{\text{ref}}} = \frac{k}{\rho C_p R^2} t^*$$

an energy balance on the wafer differential element gives the wafer temperature equation in cylindrical coordinates

$$\frac{\partial T}{\partial t} = \frac{1}{r}\frac{\partial}{\partial r}\left(r\frac{\partial T}{\partial r}\right) + \epsilon_w(1 - T^4) + q^A(r)u^A(t) + q^B(r)u^B(t) \tag{1}$$

subject to boundary conditions

$$\begin{aligned} r = 0: \quad \frac{\partial T}{\partial r} &= 0 \\ r = 1: \quad \frac{\partial T}{\partial r} &= \epsilon_e(1 - T^4) + q_e u^C(t) \end{aligned} \tag{2}$$

with

$$q^A(r) = \alpha Q^A(r) \qquad q^B(r) = \alpha Q^B(r) \qquad q_e = \alpha_e Q^C$$

and initial condition

$$T(r, t = 0) = T_0(r) \qquad r < 1. \tag{3}$$

The constants are defined in Table 1; numerical values are computed from the parameters and furnace design specifications listed in Table 2.

2.1 Radiant energy flux distributions

The lamp radiation intensity at specific points on the wafer surface will depend on the lamp power output, the distance from the wafer point to each bulb, and the angle of incidence the ray makes with the wafer surface. For our RTP system, we assume the heating lamp bulbs are arranged in three concentric circles of radius r_A, r_B, and r_C, the first two at height h above the wafer surface and the last positioned at a horizontal

Table 1: Constants of the wafer thermal dynamics PDE and boundary conditions.

Parameter	*Definition*	*Numerical Definition*	*Value*
ϵ_w	$\frac{2b\epsilon R^2 T_{\text{amb}}^3}{k\Delta_z}$	$\frac{2(5.677\times 10^{-12}\text{ J/s cm}^2\text{ K}^4)(0.7)(7.6\text{ cm})^2(300\text{ K})^3}{(0.22\text{ W/cm K})(0.05\text{ cm})}$	1.13
ϵ_e	$\frac{b\epsilon R T_{\text{amb}}^3}{k}$	$\frac{(5.677\times 10^{-12}\text{ J/s cm}^2\text{ K}^4)(0.7)(7.6\text{ cm})(300\text{ K})^3}{(0.22\text{ W/cm K})}$	0.0037
α	$\frac{R^2\epsilon}{k\Delta_z T_{\text{amb}}}$	$\frac{(7.6\text{ cm})^2(0.7)}{(0.22\text{ W/cm K})(0.05\text{ cm})(300\text{ K})}$	12.25 cm^2/W
α_e	$\frac{R\epsilon}{kT_{\text{amb}}}$	$\frac{(7.6\text{ cm})(0.7)}{(0.22\text{ W/cm K})(300\text{ K})}$	0.0806 cm^2/W
t_{ref}	$\frac{\rho C_p R^2}{k}$	$\frac{(2.3\text{ gm/cm}^3)(2.3\text{ J/gm K})(7.6\text{ cm})^2}{0.22\text{ W/(cm K)}}$	1389 s

distance w from the wafer edge so as to heat only the edge. We assume the total power output of each bank is emitted uniformly over the circular bulb arc. Given this heating lamp arrangement, the distance D from a wafer point (r,θ) to the "bulb axis" ring of lamp bank A can be written as

$$\begin{aligned} D &= \sqrt{h^2 + (r\cos\theta - r_A\cos\theta_A)^2 + (r\sin\theta - r_A\sin\theta_A)^2} \\ &= \sqrt{h^2 + r^2 + r_A^2 - 2rr_A\cos(\theta-\theta_A)}. \end{aligned}$$

If the total power output of lamp bank A is 5 kW, and the true power output is proportional to the input signal $0 \le u_A(t) \le 1$, the full-power radiation flux at wafer radius r from lamp bank A can be determined as

$$Q^A(r) = \frac{h(5,000\text{ W})}{(4\pi)(2\pi)} \int_{-\pi}^{\pi} \left[h^2 + r^2 + r_A^2 - 2rr_A\cos\theta_A\right]^{-3/2} d\theta_A$$

having assumed symmetry in the θ direction. The lamp bank locations and total bank power outputs are listed in Table 2. An identical expression is found for lamp bank B. For the total radiant energy flux at a

Table 2: Physical constant table (top) and RTP furnace design parameters (bottom).

Parameter	*Value*	*Description*
k	0.22 W/(cm K)	Si thermal conductivity
ρ	2.3 gm/cm^3	Si density
C_p	2.3 J/(gm K)	Si heat capacity
ϵ	0.7	Wafer emissivity
b	5.677×10^{-12} J/(s cm^2 K^4)	Boltzmann's constant
$T_{\rm amb}$	300 K	Reference temperature
Δ_z	0.05 cm	Wafer thickness
R	7.6 cm	Wafer radius

Lamp Bank	*Height*	*Ring Radius*	*Total Power Output*
A	2.5 cm	2 cm	5,000 W
B	2.5 cm	6 cm	20,000 W
C	0 cm	10 cm	20,000 W

point on the wafer edge we find

$$Q^C = \frac{2(20,000 \text{ W})}{(4\pi)(2\pi)} \int_0^{\theta_C^0} \frac{(R+w)\cos\theta_C - R}{[R^2 + (R+w)^2 - 2R(R+w)\cos\theta_C]^{3/2}} \, d\theta_C$$

with θ_C^0 being determined as the smallest positive solution to $\cos\theta_C = R/(R+w)$.

2.2 Nominal lamp power inputs

The "flattest" possible radiation flux distribution across the wafer that balances the radiation emitted by the wafer at its soak temperature $T^* = 1000$ K ($T = 10/3$) is determined from

$$\begin{aligned} q^A \bar{u}^A + q^B \bar{u}^B &= -\epsilon_w(1 - (10/3)^4) \\ &= 138 \text{ or } 11.3 \text{ W/cm}^2. \end{aligned}$$

The values of the dimensionless power input to each lamp bank giving a radiation flux that most closely approximates the flat power distribution calculated above is determined by minimizing the residual $\mathcal{D}$ defined

by the square of the weighted 2-norm

$$\mathcal{D} = \left\| q^A u^A + q^B u^B - 138 \right\|^2 = \int_0^1 \left[q^A u^A + q^B u^B - 138 \right]^2 r dr.$$

The condition for a global minimum of $\mathcal{D}$ translates to finding the set of nominal power inputs $(\bar{u}_A, \bar{u}_B, \bar{u}_C)$ such that

$$\begin{bmatrix} \langle q^A, q^A \rangle & \langle q^B, q^A \rangle \\ \langle q^A, q^B \rangle & \langle q^B, q^B \rangle \end{bmatrix} \begin{bmatrix} \bar{u}^A \\ \bar{u}^B \end{bmatrix} = \begin{bmatrix} \langle q^A, 138 \rangle \\ \langle q^B, 138 \rangle \end{bmatrix}$$
$$\text{and} \quad \bar{u}^C = \epsilon_e \left[(10/3)^4 - 1 \right] / q_e$$

with inner product definition

$$\langle \phi(r), \psi(r) \rangle = \int_0^1 \phi \psi \, r \, dr. \tag{4}$$

We find, for this system, the nominal lamp power inputs

$$\bar{u}^A = 0.2131 \qquad \bar{u}^B = 0.3301 \qquad \bar{u}^C = 0.2879$$

and use these values of the heating lamp power inputs to compute the nominal radiant energy flux distribution profile plotted in Fig. 1. We will now consider the problem of simulating a 60-second wafer heating cycle followed by a 60-second cooling period.

3 Eigenfunction Expansion Solution

With the model of the RTP system in hand, we turn to the problem of determining a sequence of trial functions $\{\phi_j\}_0^\infty$ that will be used to express the solution to (1) subject to the boundary and initial conditions:

$$T(r,t) = a_0(t)\phi_0 + \sum_{j=1}^{\infty} a_j(t)\phi_j(r) \tag{5}$$

$$\text{and} \qquad T^N(r,t) = \sum_{j=0}^{N} a_j(t)\phi_j(r) = \boldsymbol{\phi}\mathbf{a}. \tag{6}$$

We choose

$$\phi_0 = 1/\sqrt{\langle 1,1\rangle} = \sqrt{2},$$

a choice of trial functions that guarantees that we will be able to satisfy the wafer edge boundary conditions in the numerical techniques to be used[1]. Linearizing the wafer temperature partial differential equation (1) and the single nonlinear boundary condition of (2) at the dimensionless target soak temperature $T = 10/3$ gives[2]

$$\frac{\partial T}{\partial t} = LT + F(r,t) \tag{7}$$

subject to boundary and initial conditions

$$\begin{aligned} \frac{\partial T(0,t)}{\partial r} &= 0 \\ \frac{\partial T(1,t)}{\partial r} &= -4\epsilon_e(10/3)^3 T(1,t) + G(t) \\ T(r,0) &= T_0(r). \end{aligned} \tag{8}$$

The linear operator L and forcing functions F and G are defined as

$$\begin{aligned} L &= \frac{1}{r}\frac{\partial}{\partial r}\left(r\frac{\partial}{\partial r}\right) - 4\epsilon_w(10/3)^3 \\ F(r,t) &= \epsilon_w + 3\epsilon_w(10/3)^4 + q^A u^A + q^B u^B \\ G(t) &= \epsilon_e + 3\epsilon_e(10/3)^4 + q_e u^C \end{aligned}$$

[1] While the additional trial function ϕ_0 can be approximated *inside* the wafer domain by the complete eigenfunction sequence generated by the linearized problem, ϕ_0 does not satisfy the linearized boundary condition and so will not vanish at the wafer edge.

[2] We choose to linearize the problem at its soak temperature $T = 10/3$, since little deposition takes place at ambient conditions. Note, however, that there will be offset in the steady-state solution at all but the point of linearization.

3.1 Eigenfunctions and eigenvalues

Assuming solutions to the homogeneous problem $\dot{v} = Lv$ take the form $v = \exp(-\lambda t)\phi(r)$,

$$\begin{aligned} L\phi = \frac{1}{r}\frac{d}{dr}\left(r\frac{d\phi}{dr}\right) - 4\epsilon_w(10/3)^3\phi &= -\lambda\phi \\ r^2\phi'' + r\phi' + r^2\left[-4\epsilon_w(10/3)^3 + \lambda\right]\phi &= 0 \end{aligned}$$

where the prime denotes differentiation with respect to r, and so defining $x = r\gamma = r\sqrt{\lambda - 4\epsilon_w(10/3)^3}$ implies $x^2\phi'' + x\phi' + x^2\phi = 0$. A solution $\phi(x)$ to this form of Bessel's equation is the Bessel function of the first kind $J_n(x)$ of order $n = 0$ (Andrews, 1985; MacCluer, 1994). The boundary condition at $x = \gamma r = \gamma$ gives

$$\frac{dJ_0}{dr} = -4\epsilon_e(10/3)^3 J_0 \qquad \Longrightarrow \qquad \gamma J_1(\gamma) = 0.548 J_0(\gamma).$$

The infinite number of solutions γ_j to this nonlinear equation can be used to calculate the eigenvalues λ_j and determine the corresponding normalized eigenfunctions ϕ_j

$$\phi_j(r) = \frac{J_0(\gamma_j r)}{\sqrt{\langle J_0(\gamma_j r), J_0(\gamma_j r)\rangle}} \qquad \text{with} \qquad \lambda_j = \gamma_j^2 + 4\epsilon_w\,(10/3)^3\,. \tag{9}$$

The normalized eigenfunctions corresponding to the four smallest eigenvalues are plotted in Fig. 2. We also include a plot of the orthonormal trial functions ψ_j generated by the Gram-Schmidt procedure applied to the combined set of eigenfunctions and the single flat mode ϕ_0.

It is interesting to consider the relative contributions of each term comprising the eigenvalues (9); the values of the terms divided by t_{ref} to obtain numerical values with units sec^{-1} are tabulated in Table 3. In this table, we see that the rate of heat transfer through the wafer by conduction becomes comparable to bulk heating at about the fifth spatial mode. This means spatial perturbations of the wafer temperature can last though a significant portion of the 60-second wafer processing cycle (see the last row of Table 3, where the fraction remaining of perturbations to each mode amplitude after 20 seconds are tabulated). Because we linearize at the soak temperature, the spatial modes actually will dissipate even more slowly at the start of

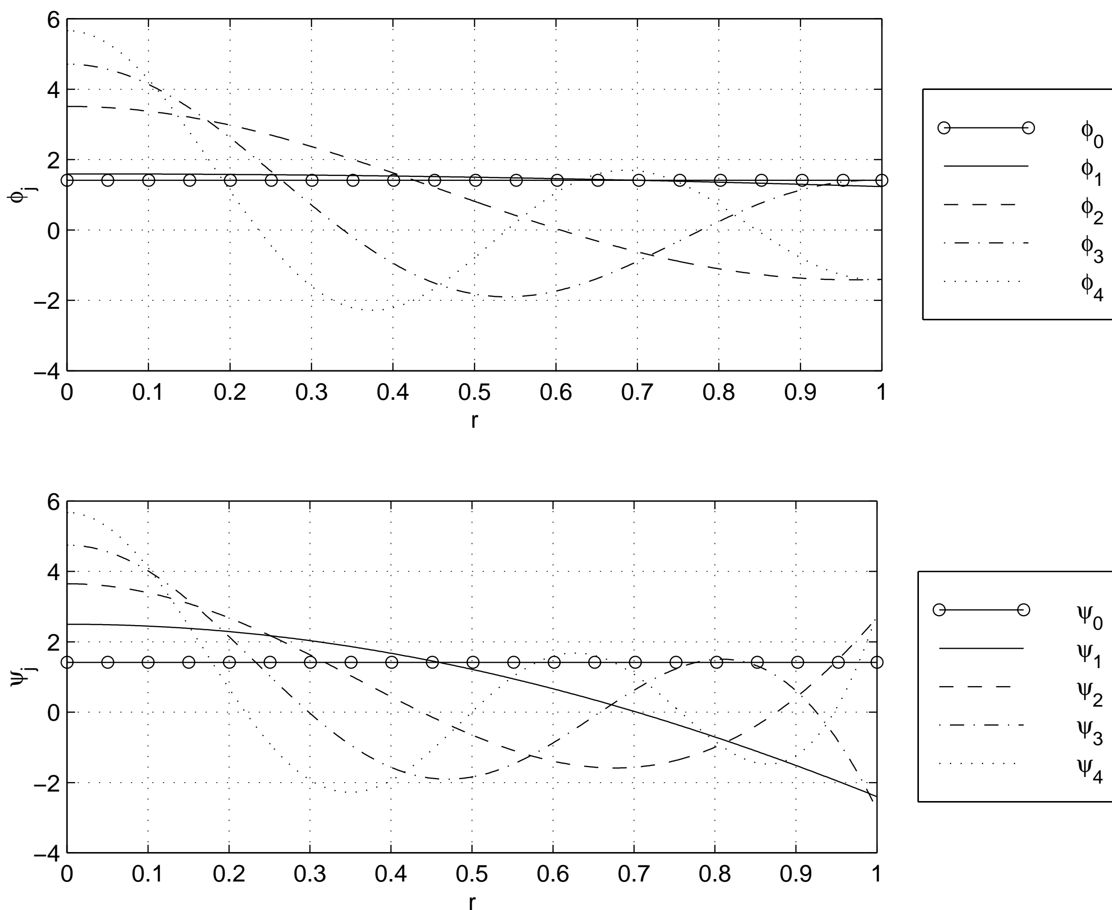

Figure 2: The first four normalized eigenfunctions ϕ_j plus the flat mode (top) and the trial functions ψ_j generated from the Gram-Schmidt orthogonalization procedure (bottom).

wafer processing; the bulk heating dynamics, however, will not change significantly because the rate of wafer heating equals the rate of radiant energy dissipation at the soak temperature. We will see that the dynamics of the linearized system gives an accurate first approximation to the nonlinear system.

3.2 Eigenfunction expansion solution

By choosing the trial functions ϕ_j, $j \geq 1$ of (5) as the eigenfunctions (9), the trial functions will satisfy the boundary condition at $r = 0$ by construction, and if we substitute (5) into the *non*homogeneous boundary

Table 3: Eigenvalues with units $\sec^{-1}$.

Mode j	0	1	2	3	4	5
$\gamma_j^2/t_{\rm ref}$	0	0.0007	0.0114	0.0362	0.0753	0.1286
$4\epsilon_w\,(10/3)^3\,/t_{\rm ref}$	0.1205	0.1205	0.1205	0.1205	0.1205	0.1205
$\exp(-20\lambda_j/t_{\rm ref})$	8.98%	8.85%	7.15%	4.35%	1.99%	0.69%

condition (8) at the wafer edge

$$\begin{aligned}\sum_{j=1}^{\infty} a_j(t)\phi_j'(1) &= -4\epsilon_e(10/3)^3\left[\sqrt{2}a_0(t)+\sum_{j=1}^{\infty}a_j(t)\phi_j(1)\right]+G(t)\\ \text{so}\qquad a_0(t) &= \frac{G(t)}{4\sqrt{2}\epsilon_e(10/3)^3}\\ &= \frac{1+3(10/3)^4+q_e u^C/\epsilon_e}{4\sqrt{2}(10/3)^3}.\end{aligned}\tag{10}$$

Furthermore, substituting (5) into the *non*homogeneous PDE (7) gives

$$\begin{aligned}\sqrt{2}\dot{a}_0+\sum_{j=1}^{\infty}\dot{a}_j\phi_j &= -4\sqrt{2}\epsilon_w(10/3)^3a_0+\sum_{j=1}^{\infty}a_jL\phi_j+F(r,t)\\ \sum_{j=1}^{\infty}\left(\dot{a}_j+\lambda_ja_j\right)\phi_j &= F(r,t)-4\sqrt{2}\epsilon_w(10/3)^3a_0-\sqrt{2}\dot{a}_0.\end{aligned}\tag{11}$$

If we now approximate the nonhomogeneous terms of the right-hand-side of (11) by the trial function expansion obtained by projecting each term onto each of the eigenfunctions ϕ_j, $j\geq 1$,

$$\begin{aligned}&F(r,t)-4\sqrt{2}\epsilon_w(10/3)^3a_0-\sqrt{2}\dot{a}_0\\ &\quad= u^A\sum_{j=1}^{\infty}\langle\phi_j,q^A\rangle\phi_j+u^B\sum_{j=1}^{\infty}\langle\phi_j,q^B\rangle\phi_j+\left[\epsilon_w+3\epsilon_w(10/3)^4-4\sqrt{2}\epsilon_w(10/3)^3a_0-\sqrt{2}\dot{a}_0\right]\sum_{j=1}^{\infty}\langle\phi_j,1\rangle\phi_j\\ &\quad= \sum_{j=1}^{\infty}\left[u^Af_j^A+u^Bf_j^B+g_j\right]\phi_j\\ &\quad= \sum_{j=1}^{\infty}M_j(t)\phi_j(r)\end{aligned}$$

with inner product definition (4). Using (11) to define a residual $\mathcal{R}(r,t)=\sum_{j=1}^{\infty}\left[\dot{a}_j+\lambda_ja_j-M_j\right]\phi_j$, $\|\mathcal{R}\|$ is minimized by setting each of the ϕ_j coefficients equal to zero (recall that the ϕ_j, $j\geq 1$ are elements of an

orthogonal sequence) and so solving the differential equations $\dot{a}_j + \lambda_j a_j - M_j(t) = 0$ we find

$$a_j(t) = a_j(0)e^{-\lambda_j t} + e^{-\lambda_j t} \int_0^t e^{\lambda_j \tau} M_j \, d\tau \qquad j \geq 1. \tag{12}$$

A particular solution for the wafer temperature profile over one processing cycle $0 \leq t \leq 2\Delta_t$ can be written as

$$\begin{aligned} a_j(t) &= a_j(0)e^{-\lambda_j t} + \frac{M_j}{\lambda_j}\left(1 - e^{-\lambda_j t}\right) && 0 \leq t < \Delta_t \\ &= a_j(\Delta_t)e^{-\lambda_j t} && \Delta_t \leq t \leq 2\Delta_t \end{aligned}$$

provided all wafer heating lamp power inputs are held constant during the powered processing segment (so $\dot{a}_0 = 0$, and a_0 and M are constant). Initial conditions are determined from

$$\begin{aligned} T(r,0) \, = \, 1 &= \sqrt{2}a_0 + \sum_{j=1}^{\infty} a_j(0)\phi_j(r) \\ \text{so} \qquad a_j(0) &= \langle 1 - \sqrt{2}a_0, \phi_j \rangle \qquad j \geq 1 \\ \text{and} \qquad a_j(\Delta_t) &= \langle \boldsymbol{\phi}\mathbf{a}(\Delta_{t_-}) - \sqrt{2}a_0, \phi_j \rangle \end{aligned} \tag{13}$$

with a_0 defined in (10). The final values of the mode amplitude coefficients during the powered segment are denoted $\mathbf{a}(\Delta_{t_-})$, a vector which includes $a_0(\Delta_{t_-})$.

3.3 Interior collocation

Alternatively, we can solve by interior collocation (Villadsen and Stewart, 1967) the nonhomogeneous PDE problem generated by defining $T = a_0\phi_0 + \hat{T}$ with $\hat{T} = \boldsymbol{\phi}\mathbf{a}$ and projecting the nonhomogeneous terms of (11) onto the ϕ_j, $j = 1, \ldots, N$:

$$\frac{\partial \hat{T}}{\partial t} = L\hat{T} + \boldsymbol{\phi}\mathbf{M}. \tag{14}$$

Here we use the vector notation for the trial functions $\boldsymbol{\phi}^{1\times N}$, mode amplitudes $\mathbf{a}^{N\times 1}$, and Fourier coefficients $\mathbf{M}^{N\times 1}$ resulting from projecting the forcing function onto the trial functions. If we write the wafer

temperature measured at a distinct point $r = r_j$ as $\hat{T}_j(t)$,

$$\hat{T}_j = \boldsymbol{\phi}(r_j)\mathbf{a} \qquad \text{or} \qquad \hat{\mathbf{T}} = \mathbf{Q}\mathbf{a}. \tag{15}$$

We choose the N collocation points r_j as the roots of ϕ_{N+1} which guarantees the invertibility of $\mathbf{Q}$, a fact crucial to computing the discretization array for the Laplacian operator[3]. The choice of collocation points also forces the residual to be orthogonal to the first N trial functions, making this interior collocation method equivalent to the eigenfunction expansion (Michelsen and Villadsen, 1981; Villadsen and Stewart, 1967). We first differentiate (15) with respect to r and rearrange the result to find:

$$\begin{aligned} \nabla^2\hat{\mathbf{T}} &= \nabla^2\mathbf{Q}\mathbf{a} \\ &= [\nabla^2\mathbf{Q}]\mathbf{Q}^{-1}\mathbf{T} \\ &= \mathbf{B}\mathbf{T} \qquad \text{with} \qquad \mathbf{B} = \left[\nabla^2\mathbf{Q}\right]\mathbf{Q}^{-1}. \end{aligned}$$

This means we can write our discretized modeling equation as

$$\begin{aligned} \frac{d\hat{\mathbf{T}}}{dt} &= \mathbf{B}\hat{\mathbf{T}} - \epsilon_w(10/3)^3\hat{\mathbf{T}} + \mathbf{Q}\mathbf{M} \\ &= -\mathbf{Q}\boldsymbol{\Lambda}\mathbf{Q}^{-1}\hat{\mathbf{T}} + \mathbf{Q}\mathbf{M} \end{aligned} \tag{16}$$

subject to initial conditions $\hat{\mathbf{T}}(t=0) = \mathbf{1}$.

Solving the collocation-discretized ODEs in time will give a solution equivalent to particular form of the eigenfunction expansion solution (12) by our choice of trial functions, since the array $\boldsymbol{\Lambda}$ consists of the eigenvalues (9) on the diagonal, and the mode amplitudes can be recovered from (15). The solution for the eigenfunction expansion/interior collocation solution is shown in Fig. 3. We now discuss its convergence properties.

[3]If $\mathbf{Q}$ was singular, we could rearrange $\mathbf{Q}$ to find row of zeros, which means it would be possible to generate a function from a nontrivial combination of the ϕ_j which either vanishes entirely (impossible) or vanishes at a number of points greater than or equal to the number of collocation points. The latter is also impossible because the function would then have some component orthogonal to the first N trial functions.

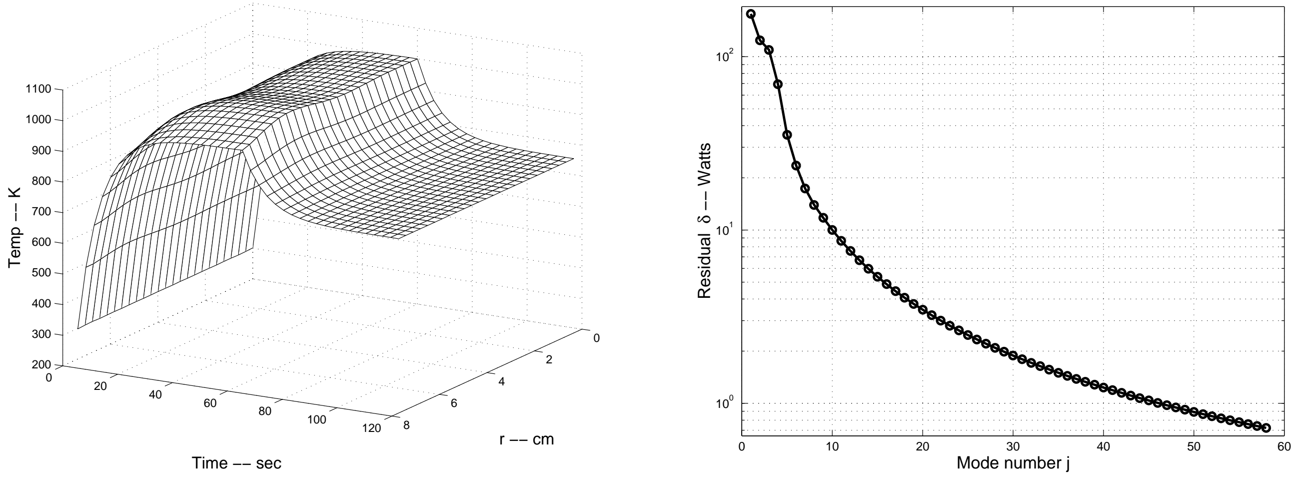

Figure 3: Eigenfunction expansion solution for $N = 58$ under nominal processing conditions (left); expected convergence behavior for the specified processing statistics.

3.4 Solution convergence

Because the eigenfunction expansion solution satisfies the nonhomogeneous boundary condition exactly, the accuracy of the truncated temperature trial function expansion (6) depends only on the accuracy with which the initial conditions, lamp radiant flux distributions, and other nonhomogeneous terms of the linearized wafer thermal dynamics differential equation (11) are represented by the trial function expansions in ϕ_j, $j = 1, \ldots, N$. Given the trial function expansion for the wafer temperature (6) and the solution defining the time-dependent mode amplitude coefficients $a_j(t)$, we can quantify the error associated with using a finite number N by computing the expected squared norm of the residual:

$$\begin{aligned}
\delta^2 &= E\left\{\|\dot{T^*}^N - L^*{T^*}^N - F^*(r^*,t^*)\|^2\right\} \\
&= \left[\left(\frac{T_{\rm amb}}{t_{\rm ref}}\right)\rho C_p \Delta_z \pi R^2\right]^2 E\left\{\|\dot{T}^N - LT^N - F(r,t)\|^2\right\} \\
&= h^2 E\left\{\|\sum_{j=1}^{N}\dot{a}_j\phi_j + 4\sqrt{2}\epsilon_w (10/3)^3 a_0 - \sum_{j=1}^{N} a_j L\phi_j - F\|^2\right\} \\
&= h^2 E\left\{\|\sum_{j=1}^{N} M_j\phi_j + 4\sqrt{2}\epsilon_w (10/3)^3 a_0 - F\|^2\right\} \\
&= h^2\left[16\epsilon_w^2 (10/3)^6 E\{a_0^2\} - 8\sqrt{2}\epsilon_w (10/3)^3 E\{a_0\} E\{\langle F,1\rangle\} + E\{\langle F,F\rangle\} - \sum_{j=1}^{N} E\left\{M_j^2\right\}\right]
\end{aligned}$$

with expectations $E\{x\}$ defined in the Appendix. The constant

$$h = \pi k T_{\rm amb} \Delta_z = 10.4 \text{ W}$$

gives the residual the same dimensions as the dimensional form of (1). Therefore, we can compare the residual magnitude directly with other physical quantities, such as the total amount of radiation emitted from the heating lamps, or the energy required to heat the wafer at a rate of 1° C/minute, a quantity that equals

$$\left(\frac{1 \text{ K}}{60 \text{ sec}}\right) \pi R^2 \Delta_z \rho C_p \approx 1\text{W}. \quad (17)$$

Representative results are shown in Fig. 3, which indicates that an eigenfunction expansion of approximately 50 terms would be required to meet the accuracy requirements specified above.

The nominal process is taken to consist of 60-second deposition runs followed by a 60-second cooling period. The initial wafer temperature is uniform and set to ambient temperature (see eqn. 13). The power inputs u^i are held constant during the soak period, and are zero when the wafer is cooled. In the expectation computations, we define the u^i to be continuous, normally-distributed, independent random variables with expectations equal to the nominal power inputs $\bar{u}^i$; numerical values of the variances for each power input were set to the square of half the expected value for each lamp bank power input. The probability distribution functions that result are shown in Fig. 4. The variable t defines the time since the start of the particular processing interval, and we take t as a uniformly distributed random variable in the range $0 \leq t < \Delta_t$ during the powered segment.

4 Mixed Collocation Solution

We now write the wafer temperature in terms of the orthonormal ψ_j, truncated after the Nth term (giving $N+1$ functions, including the flat ψ_0), or in vector notation, $\boldsymbol{\psi}^{1\times(N+1)}$ and $\mathbf{a}^{(N+1)\times 1}$ such that

$$T = \boldsymbol{\psi}\mathbf{a}. \quad (18)$$

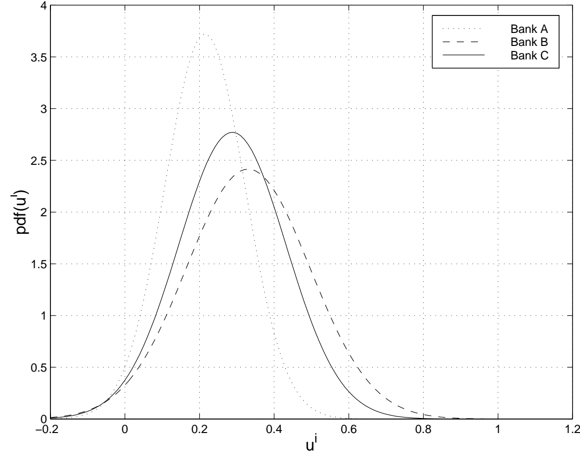

Figure 4: Probability density distribution functions describing the lamp bank power input random variables.

Once again, if the wafer temperature measured at a distinct point $r = r_j$ is $T_j(t)$, we can write $T_j = \boldsymbol{\psi}(r_j)\mathbf{a}$ or $\mathbf{T} = \mathbf{Qa}$. Differentiating with respect to r gives the discretization array for the first-order derivative

$$\frac{d\mathbf{T}}{dr} = \mathbf{AT} \qquad \text{with} \qquad \mathbf{A} = \frac{d\mathbf{Q}}{dr}\mathbf{Q}^{-1}.$$

The N interior collocation points are chosen as the roots of the last trial function used ψ_N, with one additional point placed at $r = 1$ so the wafer edge boundary condition can be satisfied. The discretized modeling equation, therefore, can be written as

$$\frac{dT_j}{dt} = \begin{cases} \mathbf{B_j T} + \epsilon_w(1 - T_j^4) + q^A(r_j)u^A + q^B(r_j)u^B & \text{(nonlinear)} \\ \\ \mathbf{B_j T} - 4\epsilon_w(10/3)^3 T_j + F(r_j, t) & \text{(linearized)} \end{cases} \tag{19}$$

for $j = 1, \ldots, N$ subject to boundary condition

$$\mathbf{A_{N+1} T} = \begin{cases} \epsilon_e(1 - T_{N+1}^4) + q_e u^C(t) & \text{(nonlinear)} \\ \\ -4\epsilon_e(10/3)^3 T_{N+1} + G(t) & \text{(linearized)} \end{cases} \tag{20}$$

and initial conditions

$$T_j = 1 \qquad j = 1, \ldots, N$$

with

$$\mathbf{T} = \begin{bmatrix} T(r_1) \\ T(r_2) \\ \vdots \\ T(r_N) \\ T(r=1) \end{bmatrix} \qquad \begin{array}{l} \mathbf{A_j} = [A_{j,1}, A_{j,2}, \ldots, A_{J,N+1}] \\ \\ \mathbf{B_j} = [B_{j,1}, B_{j,2}, \ldots, B_{J,N+1}] \end{array}$$

The boundary condition at $r = 0$ is automatically satisfied, since all the trial functions satisfy this condition.

4.1 Linearized system: computing the residual

The residual generated from the solution of the linearized, discretized wafer temperature equation (19) will live in the space spanned by the ψ_j, $j = 0, \ldots, N$ if F is replaced by the projection of F onto the ψ_j, $j = 0, \ldots, N$ (this approximation should converge to the true F for large N). Therefore, we can write

$$\mathcal{R}(r,t) = \boldsymbol{\psi}\mathbf{b} \qquad \text{or} \qquad \mathcal{R}_j = \mathcal{R}(r_j, t) = \mathbf{Q_j b}$$

and because the last column of $\mathbf{Q}$ is entirely zero save the element in the last row by our choice of collocation points, we can write the discretized residual as

$$\begin{aligned} \mathbf{0} &= \hat{\mathbf{Q}}\hat{\mathbf{b}} \\ \mathcal{R}_{N+1} &= \begin{bmatrix} \psi_0(r_{N+1}) & \psi_1(r_{N+1}) & \psi_2(r_{N+1}) & \ldots & \psi_{N-1}(r_{N+1}) & \psi_N(r_{N+1}) \end{bmatrix} b_{N+1}. \end{aligned}$$

Following Theodoropoulou et al. (1996), this implies the b_j of $\hat{\mathbf{b}}$ must be zero since the $N \times N$ top left subarray $\hat{\mathbf{Q}}$ of $\mathbf{Q}$ must be invertible by the choice of collocation points, and so the residual is simply $\mathcal{R}(r,t) = b_{N+1}\psi_{N+1}$. This collocation solution under the stated assumptions, therefore, is equivalent to the *tau* method (Gottlieb and Orszag, 1977), an implementation of Galerkin's method where the residual is made

orthogonal to the first N trial functions and the last trial function is used to satisfy the nonhomogeneous boundary condition. It is important to observe how well this equivalence holds for larger N ($N \geq 5$) for solutions where F is used directly – see Fig. 6 for the residuals corresponding to the solution of the linearized, nonhomogeneous problem. Here, we project the residual $\mathcal{R}$ onto the trial functions ψ_j to find $b_j = h\langle \mathcal{R}, \psi_j \rangle$, $j = 0, 1, \ldots$ and plot the values of the root-mean squared b_j found during the powered segment of a nominal processing cycle. We also note how the discretization error drops to nearly zero during the unpowered segment of the processing run, reflecting the accuracy possible when eigenfunctions of the linearized problem are used for trial functions.

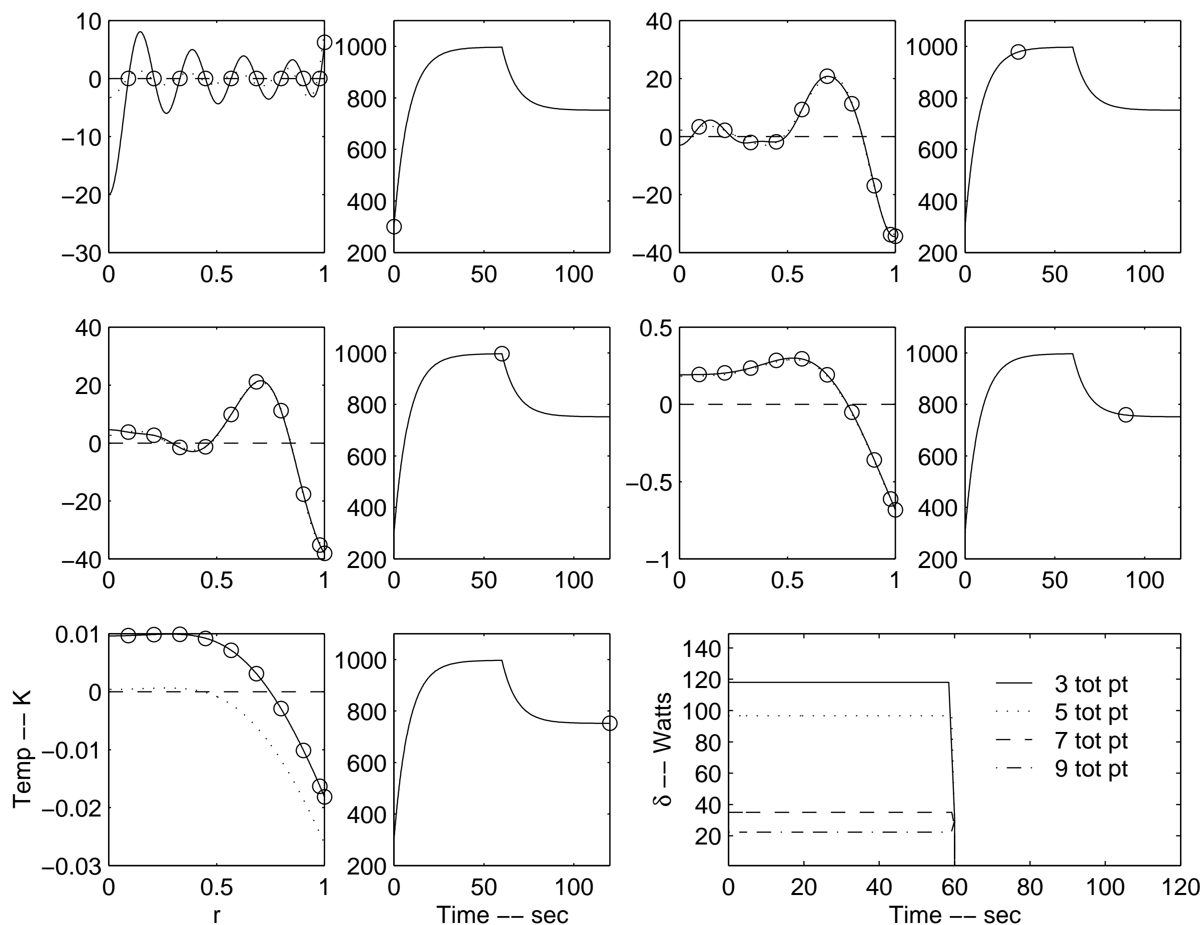

Figure 5: Linearized system collocation simulation results presented as snapshots of the full, two-minute simulation. The simulator results are shown as the wafer temperature deviation (solid curve) from the mean (dashed line) in each left-side plot, with the mean temperature marked as the point on the right-side plots of mean wafer temperature versus processing time. Collocation points are marked with circles, and the eigenfunction expansion solutions are plotted as the dotted curves. The time-dependent residual norm is plotted in the lower right corner.

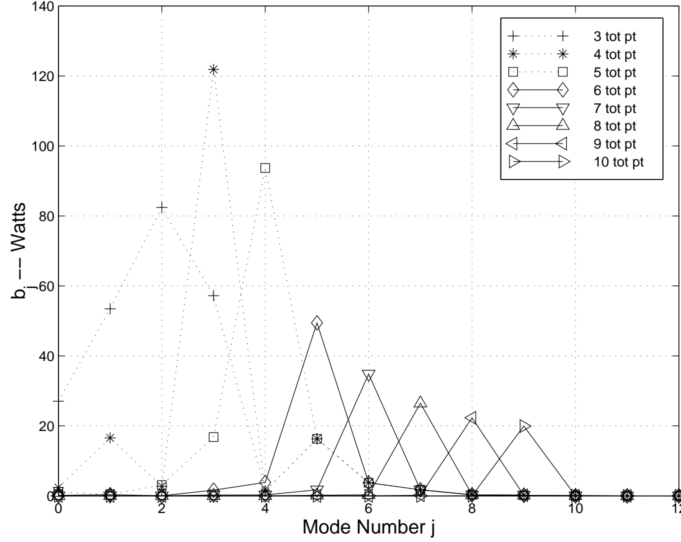

Figure 6: Expected residual mode amplitudes over the initial 60 seconds of linearized system collocation simulation.

The overall accuracy of the computed solution for the linearized problem is determined from the residual $\mathcal{R}$ norm:

$$\begin{aligned}
\delta^2 &= h^2 \|\mathcal{R}\| \\
&= h^2 \|\dot{T} - \nabla^2 T + 4\epsilon_w (10/3)^3 T - \epsilon_w - 3\epsilon_w (10/3)^4 - u^A q^A - u^B q^B\| \\
&= h^2 \|\boldsymbol{\psi}\dot{\mathbf{a}} - \nabla^2 \boldsymbol{\psi}\mathbf{a} + 4\epsilon_w (10/3)^3 \boldsymbol{\psi}\mathbf{a} - \epsilon_w - 3\epsilon_w (10/3)^4 - u^A q^A - u^B q^B\|.
\end{aligned}$$

Accurate values of the mode amplitude coefficient time derivatives are computed from (19) combined with differentiating (18) and (20) with respect to time. The norm is evaluated by numerical quadrature over the wafer domain using a discretization of the trial and forcing functions sufficiently fine to resolve the lamp radiation flux profiles. The residual, therefore, becomes a truly independent check of the numerical accuracy of the collocation technique.

From this careful residual analysis, we conclude that there is potential for generating a better set of trial functions. We take the slow, regular convergence behavior as a sign that for larger N, each additional trial function contributes only a small component, orthogonal to all higher and lower frequency modes,

to the solution convergence. The higher-frequency modes, therefore, are highly correlated with respect to solution convergence, and so can be combined in some manner to speed up the convergence of the collocation discretization solution procedure. This will be the subject of Section 5.

4.2 A least-squares-type collocation

One consequence of using a collocation technique based on a weight function that vanishes at $r = 0$ is demonstrated by the wiggles at $t = 0$ caused by the jump discontinuity of the enthalpy flux at the $r = 1$ boundary (see the top left plot of Fig. 5). This wiggling is to be expected when the wafer temperature initial conditions do not satisfy the heated edge boundary condition for $t \geq 0$. Because the weight vanishes at the wafer center, the visibly large deviation from zero at $r = 0$ does not add significantly to the discretization error; it does, however, signal potential problems of using these interpolation functions for determining the temperature at the wafer center.

Following Theodoropoulou et al. (1996), we consider the possibility of using m more collocation points than trial functions

$$\mathbf{T}^{(N+1+m)\times 1} = \mathbf{Q}^{(N+1+m)\times(N+1)}\mathbf{a}^{(N+1)\times 1}$$

to give a non-square $\mathbf{Q}$ array. Therefore, recovering the mode amplitudes from the collocation points is a solution to the least-squares problem

$$\mathbf{a} = (\mathbf{Q}^{\mathrm{T}}\mathbf{Q})^{-1}\mathbf{Q}^{\mathrm{T}}\mathbf{T}$$

(note that this solution can be used directly in defining the $\mathbf{A}$ and $\mathbf{B}$ discretization arrays). We find that for low-order discretizations, the solution computed does not pass through the collocation points, but rather, appears to be a best fit to the collocation points. This behavior is most prominent in situations such as the initial condition, where trial function fits to the solution are difficult. This collocation method results in smoother solutions since the condition of exact boundary condition solution has been relaxed (see Fig. 7).

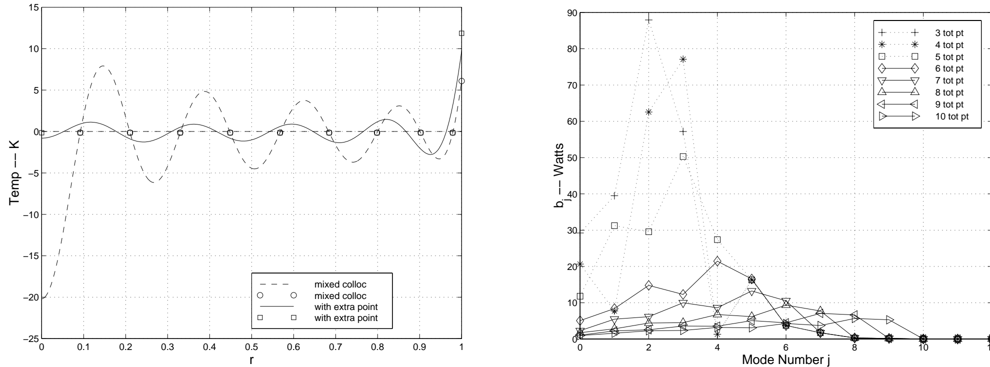

Figure 7: A comparison of the initial temperature profiles (left) and expected residual mode amplitudes over the initial 60 seconds of linearized system least-squares collocation simulation (right).

5 Optimized trial functions

The eigenfunction expansion solution procedure determines a solution in the form of a time-varying, linear combination of temperature mode shapes ϕ_j. We have shown that even though these eigenfunctions form a complete sequence and so can approximate any function living in the space spanned by the ϕ_j, the shapes of the radiant flux distribution and initial wafer temperature profiles are such that a large number of terms are required for an accurate approximation. We expect that the choice of the most efficient trial function sets should depend on a combination of the initial conditions, the length of time the system evolves, the boundary conditions, the homogeneous system eigenfunctions, and forcing functions. Therefore, by having an approximate knowledge of the initial and boundary condition statistics, and approximate expected solutions to the PDE, we can construct a better set of trial functions.

With this in mind, we propose splitting the trial function expansion (6) into two parts $T^N = T^{N-M} + T^c$. The original trial functions ψ_j, $j = 0, \ldots, N-M$ will be used in the expansion defining T^{N-M}; the remaining trial functions that form the basis of $T^c = \sum_{j=N+1-M}^{N} a_j \phi_j$ will be rearranged to improve the convergence rate of the eigenfunction expansion solution of the linearized system. Writing the latter orthonormal trial functions $\hat{\boldsymbol{\phi}}^{1\times M}$ and the mode amplitude coefficients $\hat{\mathbf{a}}^{M\times 1}$ in vector notation, we would like to find the array $\mathbf{R}$ such that if $T^c = \hat{\boldsymbol{\phi}}\hat{\mathbf{a}} = \boldsymbol{\eta}\mathbf{c}$ with

$$\eta_i = \sum_{j=1}^{M} R_{j,i}\hat{\phi}_j = \hat{\boldsymbol{\phi}}\mathbf{r_i} \qquad \text{so} \qquad \boldsymbol{\eta} = \hat{\boldsymbol{\phi}}\mathbf{R}, \tag{21}$$

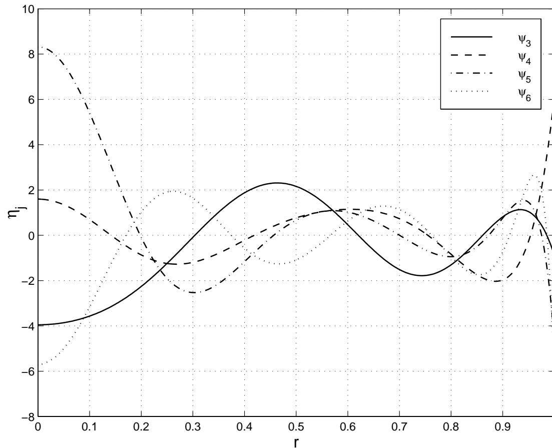

Mode j	*No. roots*	*Origin*	ϵ_j (for ϕ, η)
ψ_0	0	flat	34,201 J
ψ_1	1	ϕ_1	8,107
ψ_2	2	ϕ_2	971
ψ_3	4	η_1	616
ψ_4	4	η_2	81.5
ψ_5	5	η_3	18.6
ψ_6	6	η_4	6.2
ψ_7	7	η_5	2.3
ψ_8	8	η_6	0.9
ψ_9	9	η_7	0.3

Figure 8: Optimized trial functions and summary of the total set of optimized functions. The point where the trial function switch from the original to optimized functions was chosen as $j = 3$.

the wafer temperature component T^c would converge more quickly with η_i as trial functions compared to the original $\hat{\phi}_j$. We choose this convergence criterion over optimizing the convergence rate of the wafer temperature "acceleration" modes (Aling et al., 1997; Sirovich, 1991) – trial functions that would maximize the rate of residual convergence – because $\|\partial T/\partial t\|$ does not converge at $t = 0$ as a result of the initial conditions not satisfying the boundary condition. The need for careful accounting for the influence of the initial wafer conditions was made clear in the analysis of the linearized system eigenvalues, where it was shown how spatial features of the initial condition can persist through a significant portion of the processing cycle. We can compute the mean square of the residual norm of the wafer temperature complement T^c as

$$
\begin{aligned}
\mathcal{E}^2 &= E\left\{\|T^c\|^2\right\} = \sum_{i=1}^{M} E\left\{c_i^2\right\} \\
\text{with} \qquad c_i &= \langle \hat{\boldsymbol{\phi}}\hat{\mathbf{a}}, \eta_i \rangle \\
&= \langle \hat{\boldsymbol{\phi}}\hat{\mathbf{a}}, \hat{\boldsymbol{\phi}}\mathbf{r_i} \rangle \\
&= \hat{\mathbf{a}}^{\mathrm{T}}\mathbf{r_i}
\end{aligned}
$$

if the η_i are also orthonormal. Our new set of trial functions η_i will be computed as linear combinations of the original, the combinations determined according to the magnitude of the $\mathcal{E}_i^2$ corresponding to the

conditional variances

$$\begin{aligned} \mathcal{E}_i^2 &= E\{c_i^2\} \\ &= E\left\{\left[\hat{\mathbf{a}}^{\mathrm{T}}\mathbf{r_i}\right]^2\right\} \\ &= \mathbf{r_i}^{\mathrm{T}} E\left\{\hat{\mathbf{a}}\hat{\mathbf{a}}^{\mathrm{T}}\right\}\mathbf{r_i} \\ &= \mathbf{r_i}^{\mathrm{T}}\mathbf{C}\mathbf{r_i} \qquad \text{with} \qquad \mathbf{C} = E\left\{\hat{\mathbf{a}}\hat{\mathbf{a}}^{\mathrm{T}}\right\}. \end{aligned} \tag{22}$$

We wish to find the elements of $\mathbf{r_i}$ corresponding to the extrema of (22), subject to the condition which normalizes the $\hat{\phi}_i$:

$$\mathbf{r_i}^{\mathrm{T}}\mathbf{r_i} = 1 \tag{23}$$

and so differentiating (22) and (23) with respect to the elements $R_{j,i}$ and introducing the Lagrange multiplier λ to solve the minimization problem gives the eigenvalue problem

$$\begin{aligned} \mathbf{C}\mathbf{r_i} &= \lambda\mathbf{r_i} \\ \text{or} \qquad \mathbf{C}\mathbf{r_i} &= \epsilon_i^2\mathbf{r_i}. \end{aligned}$$

The optimized trial functions η_i are constructed with (21); the four dominant modes and their corresponding expected squared mode amplitudes ϵ_i are given in Fig. 8.

5.1 Nonlinear simulations

Having computed the optimized trial functions ψ_j, simulations of the nonlinear wafer thermal dynamics model[4] consist of computing the discretization arrays **A** and **B**, discretizing the wafer model and its nonlinear boundary condition (see equations 19 and 20), and integrating the system over the processing cycle with a second-order accurate Runge-Kutta integrator written in `MATLAB` for mixed algebraic-ordinary differential equation sets. The nonlinear boundary condition (20) is solved by Newton's method as part of the numerical

[4]Since the optimized trial functions appeared to work equally well for both the linearized and nonlinear wafer thermal dynamics models, we present only the results from the nonlinear simulations.

integration of the combined AE/ODE set. In computing the collocation solution using the optimized trial functions, we make use of the least-squares collocation procedure described earlier, since for the case of $N = 3$, we find four interior collocation points. The accuracy of the computed solution is determined from the residual norm:

$$\delta^2 = h^2 \|\boldsymbol{\psi}\dot{\mathbf{a}} - \nabla^2 \boldsymbol{\psi}\mathbf{a} - \epsilon_w(1 - (\boldsymbol{\psi}\mathbf{a})^4) - u^A q^A - u^B q^B\|.$$

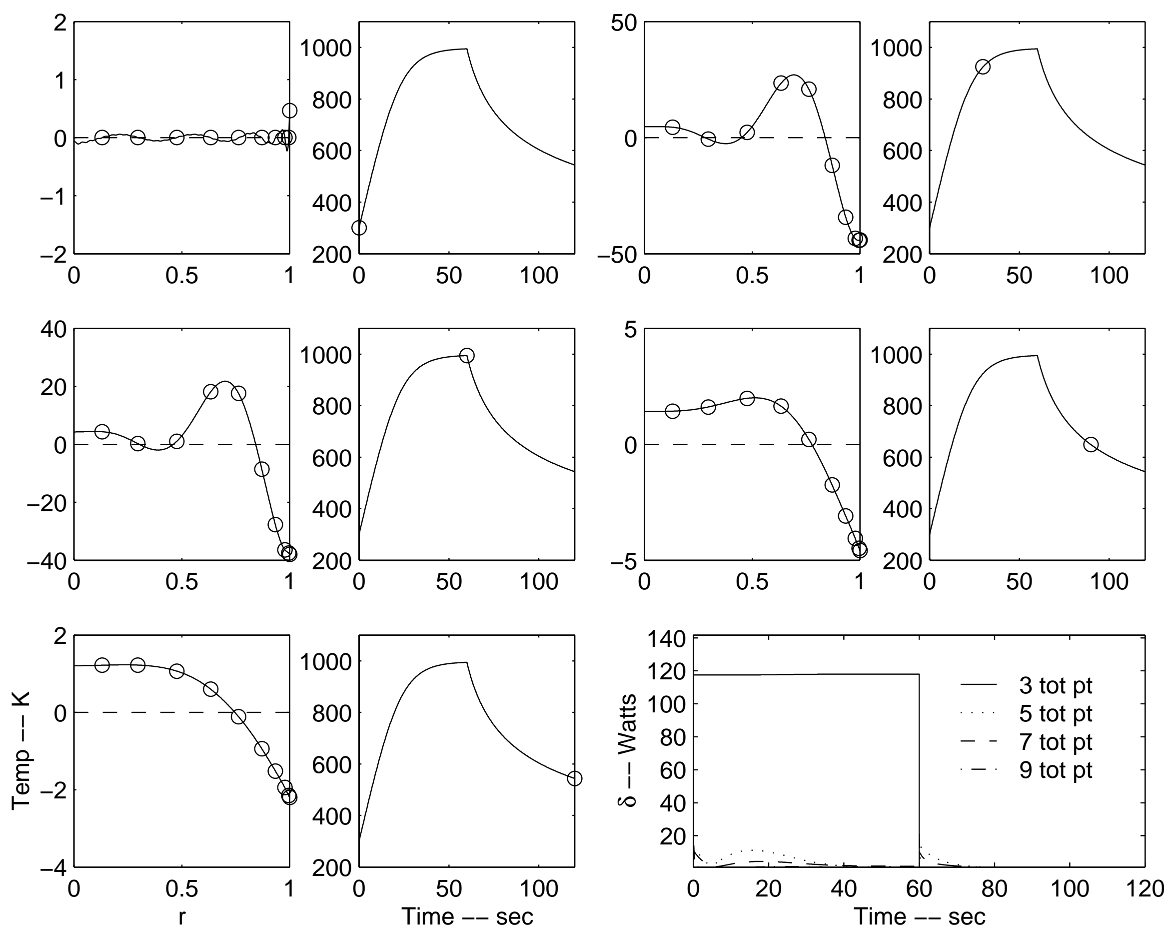

Figure 9: Optimized collocation simulation results presented as snapshots of the full, two minute simulation for the nonlinear system. The format of the plots is the same as in Fig. 5.

Simulations with the optimized trial functions show a dramatic increase in solution accuracy for $N \geq 3$ (4 total collocation points). The simulation results are displayed in Fig. 9, and a better view of the drop in residual magnitude is shown in Fig. 10. Two additional differences are seen between the linearized system/original collocation simulations and the nonlinear simulations based on the optimized trial functions:

1) a far better fit of the initial conditions can be obtained with the optimized trial functions; and 2) during the cool-down phase, while the residuals calculated for both cases are small, it appears that the radiative heat transfer nonlinearity, both in the wafer thermal dynamics equation and its boundary condition, results in a much larger temperature difference across the wafer.

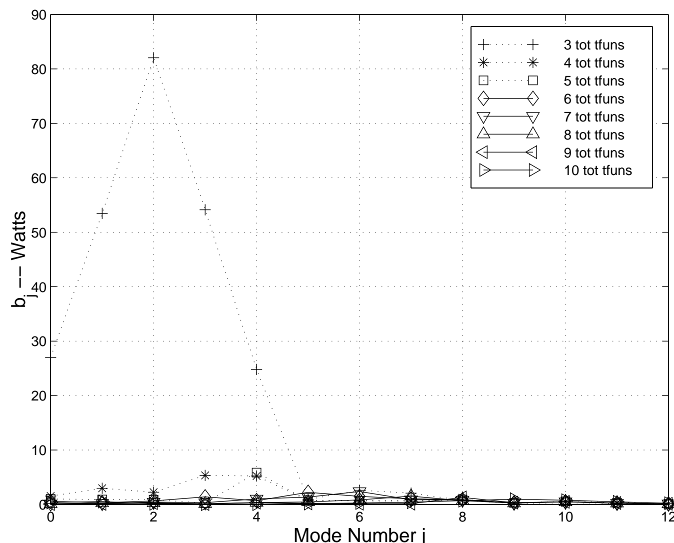

Figure 10: Expected residual mode amplitudes over the initial 60 seconds for the collocation simulation using optimized trial functions.

6 Concluding Remarks

This paper presents an efficient collocation method developed in the context of simulating a multizone RTP system. The collocation technique is based on splitting the set of linearized wafer temperature model eigenfunctions into two subsets: the first set is used as-is; the second is rearranged by computing the singular value decomposition of the wafer temperature variance, obtained explicitly from the eigenfunction expansion solution. Generating the trial function expansion in this manner leads to a sequence of trial functions featuring a nondecreasing number of zeros provided the mode number of the split point is sufficiently large. This progression of trial function zeros allows us to use the roots of the highest-order trial function as the collocation points – a least-squares-type collocation method is used in cases where the total number of collocation points exceeds the number of trial functions.

The overall effect of the collocation procedure is a sudden increase in solution accuracy when the trial function expansion switches to include the optimized trial functions. This increased accuracy is seen in Fig. 11, where a comparison is made between collocation methods based on different types of trial functions. When three trial functions are used ($N+1=3$), the polynomial and eigenfunction collocation techniques perform comparably. However, since the fourth trial function and higher modes are optimized (see Fig. 8), the residual of the new collocation procedure drops quickly relative to the polynomial and eigenfunction collocation results. The polynomial collocation results become comparable to those produced by the new procedure when 10 or more collocation points are used. Because at least three independent trial functions are required to simulate this RTP system (due to the three independently controllable lamp banks), the improved accuracy possible with the proposed collocation method in the range of four to nine trial functions should be useful for generating reduced-order RTP system models.

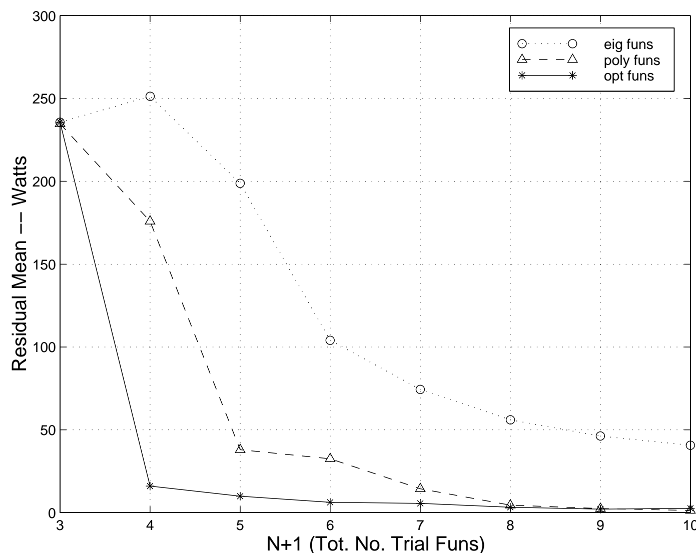

Figure 11: A final comparison of the convergence rates of collocation techniques based on the wafer thermal eigenfunctions, orthogonal polynomial sequences in r^2, and the optimized trial functions. All results are obtained from solution of the nonlinear model.

An advantage of the proposed collocation scheme is that optimized trial functions are generated prior to nonlinear simulations, a benefit that requires intricate expectation calculations. While similar, explicit calculations for more complicated modeling problems might be impractical, there is strong evidence – in particular, the excellent agreement between the results listed in the Appendix and those generated from numerical ap-

proximations as part of verifying our calculations – that suggests that good numerical approximations to the optimized trial functions can be generated.

As a final note, we see the numerical techniques developed and discussed in this paper as steps towards reducing the common problem of wiggling interpolation functions in applications of collocation based on global trial function expansions.

7 Acknowledgment

This research was supported by the National Science Foundation under grant NSF EEC 95-27576.

References

Aling, H., S. Banerjee, A. K. Bangia, V. Cole, J. L. Ebert, A. Emami-Naeini, K. F. Jensen, I. G. Kevrekidis, and S. Shvartsman 1997, Nonlinear model reduction for simulation and control of rapid thermal processing. *Proc. 1997 Amer. Control. Conf.* 2233-2238.

Aling, H., J. L. Ebert, A. Emami-Naeini, and R. L. Kosut 1996, Application of a nonlinear model reduction method to rapid thermal processing (RTP) reactors. *Proc. 1996 IFAC World Congress.*

Andrews, L. C. 1985, *Special Functions for Engineers and Applied Mathematicians* Macmillan, New York.

Belikov, S. and B. Friedland 1995, Closed-Loop Adaptive Control for Rapid Thermal Processing. *Proc. 34th IEEE CDC* 2476-2481.

Breedijk, T., T. F. Edgar, and I. Trachtenberg 1993, A Model Predictive Controller for Multivariable Temperature Control in Rapid Thermal Processing. *Proc. 1993 Amer. Control Conf.* 2980-2984.

Cole, J. V., K. L. Knutson, T. P. Merchant, and K. F. Jensen 1994, Simulation of three-dimensional flow and heat transfer in rapid thermal processing equipment. *1994 Annual AIChE Meeting.*

Dilhac, J.-M., N. Nolhier, C. Ganibal, and C. Zanchi 1995, Thermal modeling of a wafer in a rapid thermal processor. *IEEE Trans. Semicond. Manuf.* **8** 432-439.

Fukunaga, K. 1990, *Introduction to Statistical Pattern Recognition* Academic Press, Inc. San Diego. pp. 400-405.

Gottlieb, D. and S. A. Orszag 1977, *Numerical Analysis of Spectral Methods: Theory and Applications* SIAM CBMS-NSF Conf. Series in Appl. Math. **26**.

Graham, M. D. and I. G. Kevrekidis 1996, Alternative approaches to the Karhunen-Loéve decomposition for model reduction and data analysis. *Computers Chem. Enging* **20** 495-506.

Guertin, E. W. J. P. Sørensen, and W. E. Stewart 1977, Exponential collocation of stiff reactor models. *Computers Chem. Enging* **1** 197-203.

Kiether, W. J., M. J. Fordham, Seungil Yu, A. J. Silva Neto, K. A. Conrad, J. R. Hauser, F. Y. Sorrell, and J. J. Wortman 1994, Three-Zone rapid thermal processor system. *Proc. 2nd Int. RTP Conf.*, Monterey, CA, 96-101.

Larrabee, G. 1994, Flexible intelligent manufacture of microelectronic devices. *Manuf. Review* **7**, 212-226.

Lord, H. A. 1988, Thermal and stress analysis of semiconductor wafers in a rapid thermal processing oven. *IEEE Trans. Semicond. Manuf.* **1** 105-114.

MacCluer, C. R. 1994, *Boundary Value Problems and Orthogonal Expansions* IEEE Press, New York.

Merchant, T. P., J. V. Cole, K. L. Knutson, J. P. Hebb, and K. F. Jensen 1996, A systematic approach to simulating rapid thermal processing systems. *J. Electrochem. Soc.* **143**, 2035-2043.

Michelsen, M. L. and J. Villadsen 1981, Polynomial solution of differential equations. In *Foundations of Computer-Aided Chemical Process Design, Vol. I* R. S. H. Mah and W. D. Seider, Eds., 341-368.

Moslehi, M. M. 1994, Rapid thermal processing requirements for 0.35-μm IC technologies and beyond. *Mat. Res. Soc. Symp. Proc.* **342** 273-285.

Roozeboom, F. 1993, Rapid thermal processing: Status, problems, and options after the first 25 years. *Mat. Res. Soc. Symp. Proc.* **303** 149-164.

Singer, P. 1993, Rapid thermal processing: A progress report. *Semicond. International*, May, 1993, 64-69.

Sirovich, L. 1987, Turbulence and the dynamics of coherent structures, Pt. I-III. Quart. Appl. Math. **XLV**, No. 3, 561-590.

Sirovich, L. 1991, Empirical eigenfunctions and low dimensional systems. In *New Perspectives in Turbulence* L. Sirovich, Ed. Springer-Verlag New York Inc. 139-163.

Sørensen, J. P., and W. E. Stewart 1982, Collocation analysis of multicomponent diffusion and reactions in porous catalysis. *Chem. Engng Sci.* **37** 1103-1114 *and* **38** 1373.

Sorrell, F. Y., M. J. Fordham, M. C. Ozturk, and J. J. Wortman 1992, Temperature uniformity in RTP furnaces. *IEEE Trans. Electron Dev.* **39** 75-79.

Theodoropoulou, A. R. A. Adomaitis, and E. Zafiriou 1996, Model reduction for RTCVD optimization. *IEEE Semicond. Manuf.*, accepted for publication; **also** ISR TR 96-46.

Villadsen, J. V. and W. E. Stewart 1967, Solution of boundary-value problems by orthogonal collocation. *Chem. Engng Sci.* **22**, 1483-1501.

Appendix

The expected values of the mode amplitude coefficients are computed as

$$
\begin{aligned}
E\{a_0\} &= \frac{1+3(10/3)^4+q_e\bar{u}^C/\epsilon_e}{4\sqrt{2}(10/3)^3} \\
E\{a_j\} &= \frac{1}{\Delta_t\lambda_j}\left(1-e^{-\lambda_j\Delta_t}\right)\bar{a}_j(0)+\frac{E\{M_j\}}{\lambda_j}\left[1-\frac{1}{\Delta_t\lambda_j}\left(1-e^{-\lambda_j\Delta_t}\right)\right] \\
\text{with}\quad E\{M_j\} &= f_j^A\bar{u}^A+f_j^B\bar{u}^B+\epsilon_w\left[1+3(10/3)^4-4\sqrt{2}(10/3)^3E\{a_0\}\right]\langle\phi_j,1\rangle.
\end{aligned}
$$

The quantities $\bar{u}$ and $\bar{a}$ refer to the nominal lamp power inputs and initial mode amplitudes, respectively.

The expectation of the forcing function and its norm are found to be

$$
\begin{aligned}
E\{\langle F,1\rangle\} &= \frac{1}{2}\epsilon_w + \frac{3}{2}\epsilon_w(10/3)^4 + \langle q^A,1\rangle\bar{u}^A + \langle q^B,1\rangle\bar{u}^B \\
E\{\langle F,F\rangle\} &= \frac{1}{2}\left[\epsilon_w + 3\epsilon_w(10/3)^4\right]^2 + 2\left[\epsilon_w + 3\epsilon_w(10/3)^4\right]\left[\langle q^A,1\rangle\bar{u}^A + \langle q^B,1\rangle\bar{u}^B\right] \\
&\quad +\langle q^A,q^A\rangle(\sigma_{uA}^2 + (\bar{u}^A)^2) + 2\langle q^A,q^B\rangle\bar{u}^A\bar{u}^B + \langle q^B,q^B\rangle(\sigma_{uB}^2 + (\bar{u}^B)^2)
\end{aligned}
$$

The elements of the variance array are computed from

$$
\begin{aligned}
E\{a_j^2\} &= E\left\{a_j^2(0)\right\}\frac{1-e^{-2\lambda_j\Delta_t}}{2\Delta_t\lambda_j} + E\{a_j(0)M_j\}\frac{1-2e^{-\lambda_j\Delta_t}+e^{-2\lambda_j\Delta_t}}{\Delta_t\lambda_j^2} \\
&\quad +E\{M_j^2\}\frac{2\Delta_t\lambda_j - 3 + 4e^{-\lambda_j\Delta_t} - e^{-2\lambda_j\Delta_t}}{2\Delta_t\lambda_j^3} \\
E\{a_ja_k\} &= E\left\{a_j(0)a_k(0)\right\}\frac{1-e^{-(\lambda_j+\lambda_k)\Delta_t}}{\Delta_t(\lambda_j+\lambda_k)} + \frac{E\{a_k(0)M_j\}}{\lambda_j}\left[\frac{1-e^{-\lambda_k\Delta_t}}{\Delta_t\lambda_k} - \frac{1-e^{-(\lambda_j+\lambda_k)\Delta_t}}{\Delta_t(\lambda_j+\lambda_k)}\right] \\
&\quad +\frac{E\{a_j(0)M_k\}}{\lambda_k}\left[\frac{1-e^{-\lambda_j\Delta_t}}{\Delta_t\lambda_j} - \frac{1-e^{-(\lambda_j+\lambda_k)\Delta_t}}{\Delta_t(\lambda_j+\lambda_k)}\right] \\
&\quad +\frac{E\{M_jM_k\}}{\lambda_j\lambda_k}\left[1 - \frac{1-e^{-\lambda_j\Delta_t}}{\Delta_t\lambda_j} - \frac{1-e^{-\lambda_k\Delta_t}}{\Delta_t\lambda_k} + \frac{1-e^{-(\lambda_j+\lambda_k)\Delta_t}}{\Delta_t(\lambda_j+\lambda_k)}\right]
\end{aligned}
$$

with

$$
\begin{aligned}
E\{M_j^2\} &= (f_j^A)^2(\sigma_{uA}^2 + (\bar{u}^A)^2) + (f_j^B)^2(\sigma_{uB}^2 + (\bar{u}^B)^2) + 2\bar{u}^A\bar{u}^B f_j^A f_j^B + \big[(1+3(10/3)^4)^2 \\
&\quad -8\sqrt{2}(10/3)^3(1+3(10/3)^4)E\{a_0\} + 32(10/3)^6E\{a_0^2\}\big]\epsilon_w^2\langle\phi_j,1\rangle^2 \\
&\quad +2\epsilon_w[1+3(10/3)^4 - 4\sqrt{2}(10/3)^3E\{a_0\}]\langle\phi_j,1\rangle(\bar{u}^A f_j^A + \bar{u}^B f_j^B) \\
E\{M_jM_k\} &= (\sigma_{uA}^2 + (\bar{u}^A)^2)f_j^A f_k^A + (\sigma_{uB}^2 + (\bar{u}^B)^2)f_j^B f_k^B + 32\epsilon_w^2(10/3)^6E\{a_0^2\}\langle\phi_j,1\rangle\langle\phi_k,1\rangle \\
&\quad +\bar{u}^A f_j^A\left(\bar{u}^B f_k^B + \epsilon_w[1+3(10/3)^4 - 4\sqrt{2}(10/3)^3E\{a_0\}]\langle\phi_k,1\rangle\right) \\
&\quad +\bar{u}^B f_j^B\left(\bar{u}^A f_k^A + \epsilon_w[1+3(10/3)^4 - 4\sqrt{2}(10/3)^3E\{a_0\}]\langle\phi_k,1\rangle\right) \\
&\quad +\epsilon_w[1+3(10/3)^4]\langle\phi_j,1\rangle\big(\bar{u}^A f_k^A + \bar{u}^B f_k^B + \epsilon_w[1+3(10/3)^4 - 4\sqrt{2}(10/3)^3E\{a_0\}]\langle\phi_k,1\rangle\big) \\
&\quad -4\sqrt{2}\epsilon_w(10/3)^3E\{a_0\}\langle\phi_j,1\rangle\left(\bar{u}^A f_k^A + \bar{u}^B f_k^B + \epsilon_w[1+3(10/3)^4]\langle\phi_k,1\rangle\right)
\end{aligned}
$$

$$
\begin{aligned}
E\{a_0^2\} &= \frac{1}{32(10/3)^6}\left[\left[1+3(10/3)^4\right]^2 + 2\left[1+3(10/3)^4\right]\frac{q_e\bar{u}^C}{\epsilon_e} + \frac{q_e^2}{\epsilon_e^2}\left[\sigma_{uC}^2 + (\bar{u}^C)^2\right]\right] \\
E\{a_j(0)a_k(0)\} &= (1-2\sqrt{2}E\{a_0\} + 2E\{a_0^2\})\langle\phi_j,1\rangle\langle\phi_k,1\rangle \qquad \text{for all } j,\ k \\
E\{a_0 a_j(0)\} &= (E\{a_0\} - \sqrt{2}E\{a_0^2\})\langle\phi_j,1\rangle \\
E\{M_j a_k(0)\} &= E\{a_k(0)\}\left(\bar{u}^A f_j^A + \bar{u}^B f_j^B + \epsilon_w[1+3(10/3)^4]\langle\phi_j,1\rangle\right) \\
&\quad -4\sqrt{2}\epsilon_w(10/3)^3\langle\phi_j,1\rangle E\{a_0 a_k(0)\} \qquad \text{for all } j,\ k
\end{aligned}
$$